sustainability

MDPI

Article

Modelling and Performance Assessment of a Ground-Coupled Ammonia Heat Pump System: The EMPEC Ustka Case Study

Ireneusz Zagrodzki [1], Mateusz Bryk [2], Piotr Józef Ziółkowski [2,*], Tomasz Kowalczyk [2], Pedro Jesus Cabrera Santana [3] and Janusz Badur [2]

[1] EMPEC Ustka, Bałtycka 5a Street, 76-270 Ustka, Poland; i.z@wp.pl
[2] Energy Conversion Department, Institute of Fluid Flow Machinery Polish Academy of Sciences, Fiszera 14 St., 80-231 Gdańsk, Poland; mbryk@imp.gda.pl (M.B.); tkowalczyk@imp.gda.pl (T.K.); jb@imp.gda.pl (J.B.)
[3] Mechanical Engineering Department, Campus de Tafira s/n, University of Las Palmas de Gran Canaria, 35017 Las Palmas de Gran Canaria, Spain; pedro.cabrerasantana@ulpgc.es
* Correspondence: pjziolkowski@imp.gda.pl

Abstract

This study evaluates the feasibility of using a ground-coupled ammonia heat pump as a heat source for the district heating system in Ustka, Poland. A three-dimensional transient thermal model of a 122-borehole field was developed in ANSYS 2023 R1 using local geological data and hourly meteorological inputs. Three extraction loads—0.50, 0.75, and 1.00 MW—were analysed, together with regeneration periods of one month (August) and six months following the heating season. Ground temperatures were assessed across all geological layers down to 250 m. The simulations show that each of the tested loads leads to a noticeable and lasting reduction in ground temperature. For 1.00 MW, the temperature in the main heat-exchange layers remains more than 2 K below the initial value even after six months of regeneration. At 0.75 MW the deficit is smaller but still persists in the layers that dominate heat transfer. Even the 0.50 MW scenario does not return to thermal balance: the active layers stay more than 1 K cooler after the regeneration period, indicating cumulative long-term cooling. Although the model includes standard engineering simplifications, the large-scale thermal behaviour is consistent across all scenarios. The analysis shows that the analysed GSHP (ground-source heat pump) configuration cannot serve as a primary heat source for the Ustka network in the analysed configuration. Alternative low-emission solutions, such as air-source heat pumps supported by renewable electricity, are more suitable for this site.

Keywords: sustainable energy system; decarbonization; ground-source heat pump; CFD simulation; thermal response of geological layers; transient heat transfer

Academic Editor: Marco Noro

Received: 5 December 2025
Revised: 23 January 2026
Accepted: 30 January 2026
Published: 7 February 2026

1. Introduction

The decarbonization of district heating networks is one of the central challenges in the transition toward sustainable and climate-neutral energy systems. Across Europe, heating remains a major source of greenhouse gas emissions, and integrating renewable heat technologies is increasingly recognised as essential for reducing reliance on fossil fuels. Among available solutions, heat pumps using environmental energy from air or ground sources have gained particular attention due to their high efficiency and compatibility with low-carbon strategies. Ground-source heat pumps (GSHPs), in particular, benefit from the stable thermal conditions of the subsurface, which allow efficient operation even during periods of low outdoor temperatures.

The performance and feasibility of GSHP systems depend on the thermophysical characteristics of the soil, the design of the ground heat exchanger (GHE), and the long-term thermal balance between extraction and regeneration. Several studies have analysed GSHP efficiency, soil temperature variation, and thermo-economic performance across different climates and configurations. For example, Demir et al. [1] emphasised that soil thermal conductivity, burial depth, and seasonal ground temperature variability strongly affect system efficiency and optimal GHE design. Lucia et al. [2] highlighted the importance of transient thermodynamic analysis and exergy-based optimisation, suggesting that GSHP systems require modelling beyond steady-state assumptions. More recent work by Aresti et al. [3] demonstrated that GSHPs can outperform air-source heat pumps (ASHPs) from an environmental perspective, but only when geological conditions and heating loads are favourable.

At the same time, the operation of GSHP systems must be viewed within the broader context of sustainable and resilient energy systems. The integration of renewable energy sources presents challenges related to variability and system stability. High shares of renewables require advanced flexibility and energy storage, as evidenced by studies on flywheel energy storage systems (FESSs), which provide rapid-response balancing services and support grids with significant renewable penetration [4]. Similarly, system-level analyses using Smart Energy System methodologies show that large-scale renewable integration, such as full electrification of transport or heating, requires coordinated operation of energy generation, storage, and grid stability measures [5]. These findings underline that technological performance must be evaluated not only at the device scale (e.g., GSHP COP) but also within the wider energy system framework, including variability management and economic feasibility.

The viability of renewable technologies is also shaped by regulatory and market conditions. Studies examining renewable energy support schemes, such as the work of Rosales-Asensio et al. [6] on Spanish tariff structures, show that the effectiveness and cost-efficiency of integrating renewables depend heavily on well-designed policy mechanisms, particularly in electricity markets with marginal pricing. These insights are relevant for GSHP deployment in district heating, where electricity price volatility, market support frameworks, and operating strategies can significantly influence techno-economic performance.

Despite the extensive literature, important knowledge gaps remain regarding the scalability of GSHP systems for high-temperature district heating. Most existing research focuses on small-scale buildings, idealised or single-borehole models, or low-temperature heating regimes.

A comprehensive evaluation that integrates geological conditions, heat pump performance and economic factors is required, as each of these components influences the feasibility of the system. The present study addresses this gap by evaluating the feasibility of integrating ground-source and air-source heat pumps into a municipal district heating network, using a combination of fully transient 3D simulations of a 122-borehole field and an optimisation model including GSHP, ASHP, CHP, and thermal storage. The analysis aims to determine the realistic extractable heat potential of the ground, quantify its sustainability under local geological conditions, and assess the implications for the design of a hybrid district heating system.

This study quantifies the extractable heat under the local geological and climatic conditions and evaluates its implications for the configuration of the district heating system. In a broader perspective, the findings contribute to the ongoing discussion on the role of GSHPs in urban heating decarbonization. The results demonstrate that assessing ground thermal regeneration is essential for the proper sizing of heat pump systems in district heating applications.

Despite extensive research on ground-source heat pumps, several critical gaps remain concerning their applicability in large-scale district heating systems. Existing studies predominantly focus on small building-level applications, assume favourable geothermal conditions, or rely on simplified analytical models of borehole heat transfer. Only a limited number of publications evaluate the long-term thermal depletion of the ground under high extraction loads, and even fewer combine realistic geological constraints with high-temperature ammonia heat pumps (up to 95–100 °C) operating in district heating networks.

Furthermore, previous modelling efforts rarely integrate three-dimensional, transient simulations of a dense borehole field with system-level techno-economic optimisation involving CHP units, thermal storage, and air-source heat pumps. As a result, the practical limits of GSHP scalability in real municipal conditions remain poorly understood, especially in regions with relatively low geothermal gradients.

The present study addresses these gaps by providing a fully integrated assessment of a 1 MW ammonia heat pump coupled with a 122-borehole field, combining detailed 3D transient subsurface modelling with the optimisation of hybrid system operation.

Numerical modelling of borehole heat exchangers and long-term thermal imbalance has been widely addressed in the literature; the present study applies established modelling approaches to a site-specific feasibility assessment.

An independent techno-economic optimisation study was conducted for the same district heating system using operational data from 2021 to 2022. The analysis showed that, for the available plot area (≈3.5 ha) and borehole depth of 150 m, the ground heat exchanger could be sustainably loaded at approximately 100 kW in long-term operation, while higher extraction rates required extended seasonal regeneration. These findings support the conclusions drawn from the numerical simulations presented in this paper.

In this paper, the integration of GSHP within the district heating system is therefore addressed through the feasibility of the ground heat source itself, rather than through an explicit simulation of the heat pump cycle or network hydraulics.

2. Methods

2.1. Basic Assumptions

To keep the simulations computationally feasible while preserving the large-scale behaviour of the borehole field, several modelling simplifications were adopted. The U-tubes were not modelled explicitly; instead, each borehole was represented as a single cylindrical volume with an equivalent heat-exchange surface. It was performed in order to reduce computational complexity. Instead, heat extraction was imposed through an equivalent cylindrical boundary. This representation does not aim to reproduce borehole thermal resistance or fluid temperature variation but serves as a modelling construct to analyse long-term ground thermal behaviour and interaction between neighbouring boreholes.

The choice of the equivalent diameter was guided by the objective of distributing the imposed heat extraction over a boundary with an effective perimeter comparable to that of the U-tube. The authors acknowledge that this approximation affects borehole-scale thermal details but does not alter the qualitative conclusions regarding long-term ground cooling and regeneration, which are the focus of this feasibility study. As a consequence, the model does not reproduce the detailed thermal resistance of the borehole or the temperature stratification of the circulating fluid. The results therefore reflect the response of the ground mass rather than the internal behaviour of the borehole.

Heat transfer in the subsurface was assumed to occur purely by conduction, and groundwater flow was not included. Neglecting groundwater advection represents a conservative assumption, as advective heat transport would generally enhance thermal regeneration and mitigate long-term temperature depletion rather than intensify it. The

geological layers were treated as homogeneous, with constant thermal properties taken from hydrogeological reports. Although these assumptions neglect local heterogeneity and advective heat transport, they are appropriate for evaluating the long-term thermal balance of a borehole field, which is governed primarily by conduction.

The surface boundary conditions were based on hourly meteorological data for air temperature and solar irradiance. Effects such as vegetation, snow cover, shading, or seasonal soil moisture variations were not included. The side and bottom boundaries of the model were placed sufficiently far from the borehole field to avoid numerical interference; however, they still represent an approximation of the actual lateral and vertical thermal exchange.

Finally, layer temperatures reported in the results correspond to volume-averaged values, which smooth out local fluctuations but provide a robust measure of bulk thermal behaviour. Overall, while the model contains typical simplifications used in engineering practice, it captures the dominant mechanisms governing long-term ground cooling and is adequate for evaluating the feasibility of the proposed GSHP configuration.

A view of the plot of land under consideration for the installation of a ground-source heat pump is shown in Figure 1. Figure 2 shows the division of the ground by depth and the construction of the U-tube used in the borehole.

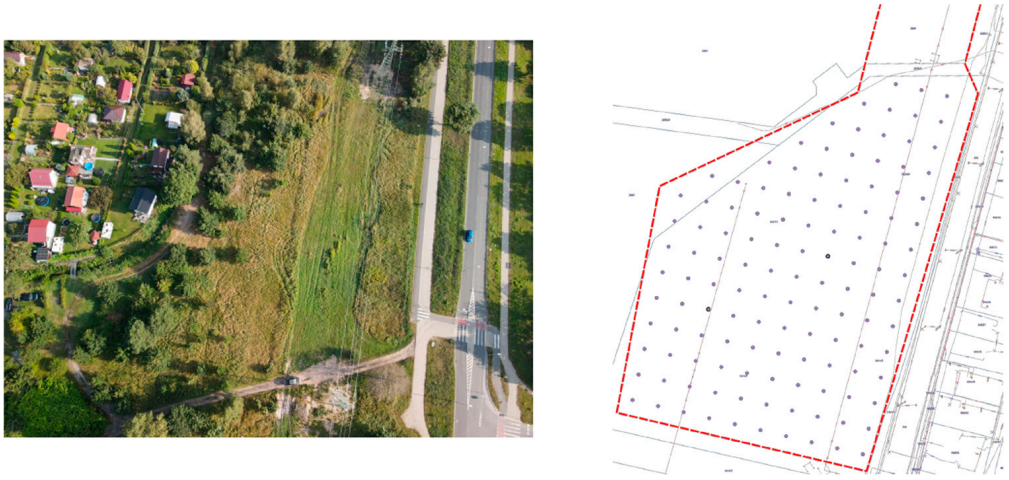

Figure 1. View of the plot under consideration for the installation of a ground-source heat pump [7].

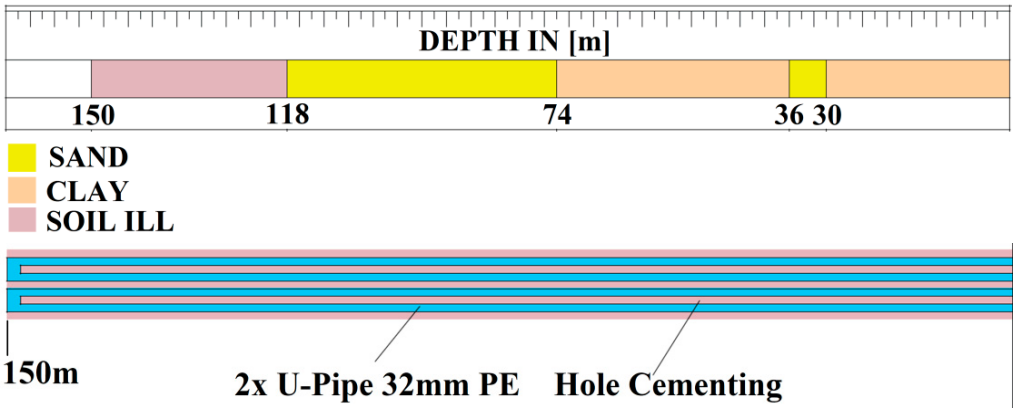

Figure 2. View of the soil layer and the structure of the hole. The figure provides a schematic representation of the geological stratification; layer depths are given in Table 1.

Table 1. Properties of soil layer [8–10].

Layer	Thermal Conductivity k [W/mK]	Layer Thickness
Clay	1.6	30
Sand	2.4	6
Clay	1.6	38
Sand	2.4	44
Stiff clay	1.6	32

Based on the geological cross-section, the following geological profile is assumed in the subsoil:

0.0–30.0 clay
30.0–36.0 sand
36.0–74.0 clay
74.0–118.0 sand
118.0–150 loam (Miocene)

The following assumptions were made for further analyses:

- Hole depth: 150 m;
- Distance between holes: 15 m;
- Exchanger type: double U-tube 32 × 3.0 mm;
- Minimum return temperature: 0 °C.

Ammonia was selected as the refrigerant due to its widespread application in large-scale, high-temperature heat pumps for district heating systems. In the present study, the thermodynamic cycle of the heat pump is not explicitly modelled; instead, the analysis focuses on the long-term thermal behaviour and feasibility of the ground heat source.

2.2. Three-Dimensional Model

Based on the information presented in report [11] and the data provided in [7], a numerical model of the plot with a surface area of 30,000 m^2 was developed. The model included 122 vertical boreholes, each with a depth of 150 m. The number of boreholes (122) and their spacing were fixed by the available land area and preliminary design constraints and were not treated as optimisation variables. To capture the effects of ground cooling and thermal regeneration, the computational domain was extended by an additional 100 m in depth and 300 m beyond the plot boundary in all horizontal directions. The geological geometry was discretized into layers according to the stratigraphy described in [11], as shown in Figure 3.

References [7,11] are local planning and hydrogeological reports used exclusively as sources of site-specific input data.

Due to the small diameters of both the boreholes and the U-pipes relative to the overall model geometry, a geometric simplification was introduced. The U-pipe geometry was omitted and replaced by a single cylindrical borehole representation with a diameter equal to four times the diameter of the U-pipes. This approach preserves the same effective heat-exchange surface area while substantially reducing the complexity of the numerical model. The original borehole diameter was retained, and the resulting simplified borehole configuration is shown in Figure 3. Figure 3 is schematic and not drawn to scale; characteristic dimensions are given in metres.

The borehole spacing and layout were adopted from the preliminary design and were not optimised within the scope of this feasibility study:

Layer I—0–30 m;
Layer II—30–36 m;
Layer III—36–74 m;

Layer IV—74–118 m;
Layer V—118–150 m;
Layer VI—150–160 m;
Layer VII—160–250 m.

In Figure 3c the inner frame marks the borehole field area, while the outer frame represents the extended computational domain used to reduce boundary effects.

Although the borehole heat exchangers extend to 150 m, the numerical domain was extended to 250 m to reduce boundary effects. Layers VI and VII serve as a thermal buffer and are not directly involved in heat extraction.

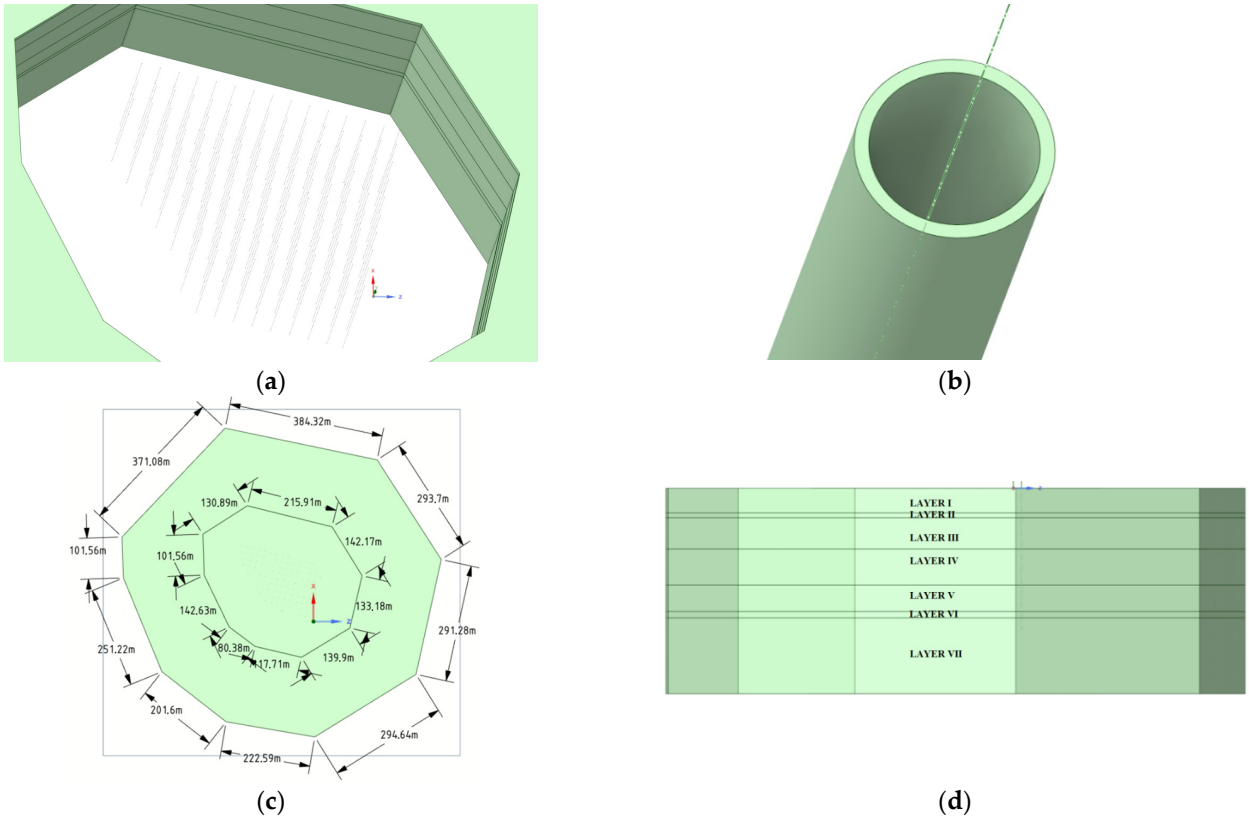

Figure 3. View of land domain and boreholes with pipes: (**a**) view of location of pipes in ground, (**b**) pipe simplification, (**c**) main dimensions of analysed soil, and (**d**) layers of analysed soil. Colours are used only to distinguish individual geological layers and do not represent horizontal variability of material properties.

2.3. Mathematical Model

The heat exchange between the ground heat exchanger and the surrounding soil was modelled as a transient heat-transfer process in a solid medium using the ANSYS Mechanical Transient Thermal module. The calculations accounted for thermal conduction in the multilayer geological structure, time-dependent boundary conditions at the ground surface, and imposed heat fluxes on the borehole walls corresponding to the operating conditions of the heat pump. The heat transfer in the ground is described by the transient form of Fourier's heat conduction equation [12–14]:

$$\rho c_p \frac{\partial T}{\partial t} = \nabla \cdot (k \nabla T)$$

where

$T(x,t)$ —temperature as a function of time and spatial coordinates;

ρ —soil density;
c_p—specific heat;
k—thermal conduction.

At the ground surface (z = 0), a time-dependent Dirichlet boundary condition was applied in the following form:

$$T(z = 0, t) = T_{surf}(t),$$

where $T_{surf}(t)$ is the hourly averaged ground surface temperature derived from meteorological data for Ustka City (Figure 4). No additional surface heat-flux boundary was imposed.

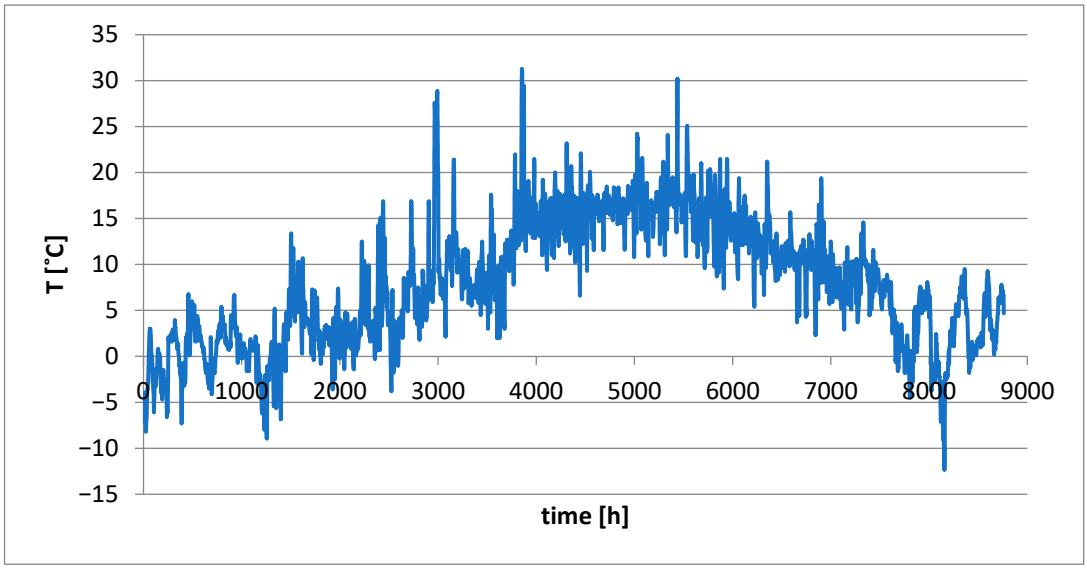

Figure 4. Hourly averaged outdoor air temperature for Ustka in the year 2023 [15].

The material parameters were assigned individually to each soil layer in accordance with the geological profile.

For the thermal simulations of the ground heat exchanger (GHE) field, the total thermal load $\dot{Q}_{tot}$ assigned to the ammonia heat pump was uniformly distributed among the 122 vertical boreholes. The heat extraction rate for a single borehole was therefore defined as follows:

$$\dot{Q}_{BH} = \frac{\dot{Q}_{tot}}{N_{BH}}$$

where
$\dot{Q}_{tot}$—heat extraction rate of a single borehole [W];
$\dot{Q}_{BH}$—total thermal load applied to the GHE field [W];
N_{BH}—number of holes: 122.

The heat extraction boundary condition was applied as a uniform heat flux on the cylindrical wall surface of each borehole. The external wall area of a single borehole was calculated as follows:

$$A_{BH} = 2\pi r_{BH} L_{BH}$$

where
r_{BH}—borehole radius;
L_{BH}—borehole depth: 150 m.

The resulting heat flux assigned to each borehole:

$$q'' = \frac{\dot{Q}_{BH}}{A_{BH}}$$

The flux q'' was imposed directly on the borehole wall as a constant heat flux boundary condition, independent of depth.

At the ground surface, time-varying boundary conditions were imposed, including the ambient air temperature and the incoming solar radiation flux (ITH):

$$-k\frac{\partial T}{\partial n} = q_s(t)$$

where

$$q_S(t) = \alpha_s ITH(t)$$

The ground surface temperature was prescribed according to the time-dependent profile derived from the meteorological data. Solar irradiance (ITH) was used only to derive the surface temperature profile and was not applied as an independent Neumann-type heat-flux boundary condition in the numerical model.

Using a constant heat flux allows direct comparison of different extraction scenarios and provides a conservative estimate of long-term ground cooling, independent of short-term operational fluctuations.

2.4. Thermal Properties and Boundary Conditions

For each geological layer, the corresponding thermal conductivity values were assigned, as listed in Table 1. The initial temperature was defined as a function of depth based on the geothermal profile (approximately 11 °C at a depth of 250 m) [16–20]. Figure 5 represents hourly averaged total solar irradiance on a horizontal plane (ITH) for Ustka throughout 2023 according to [21].

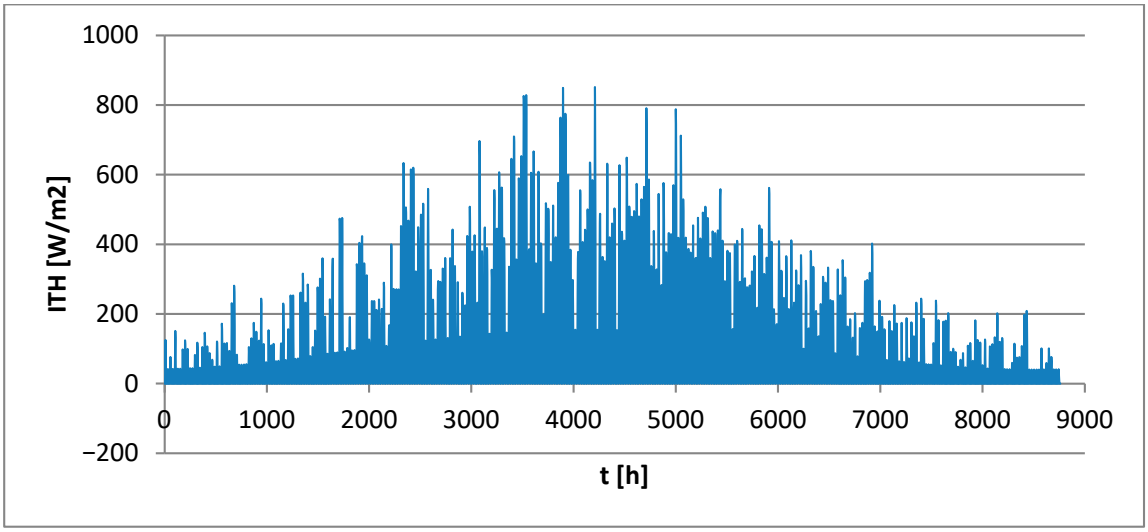

Figure 5. Hourly averaged total solar irradiance on a horizontal plane (ITH) for Ustka in 2023 [21].

Figure 6 shows the initial ground temperature assumed in the analysis: (a) central cross-section, (b) depth 112.5 m.

To simulate ground thermal depletion, three heat extraction capacities of the ground heat exchanger were considered:

I—1.00 MW;
II—0.75 MW;
III—0.50 MW.

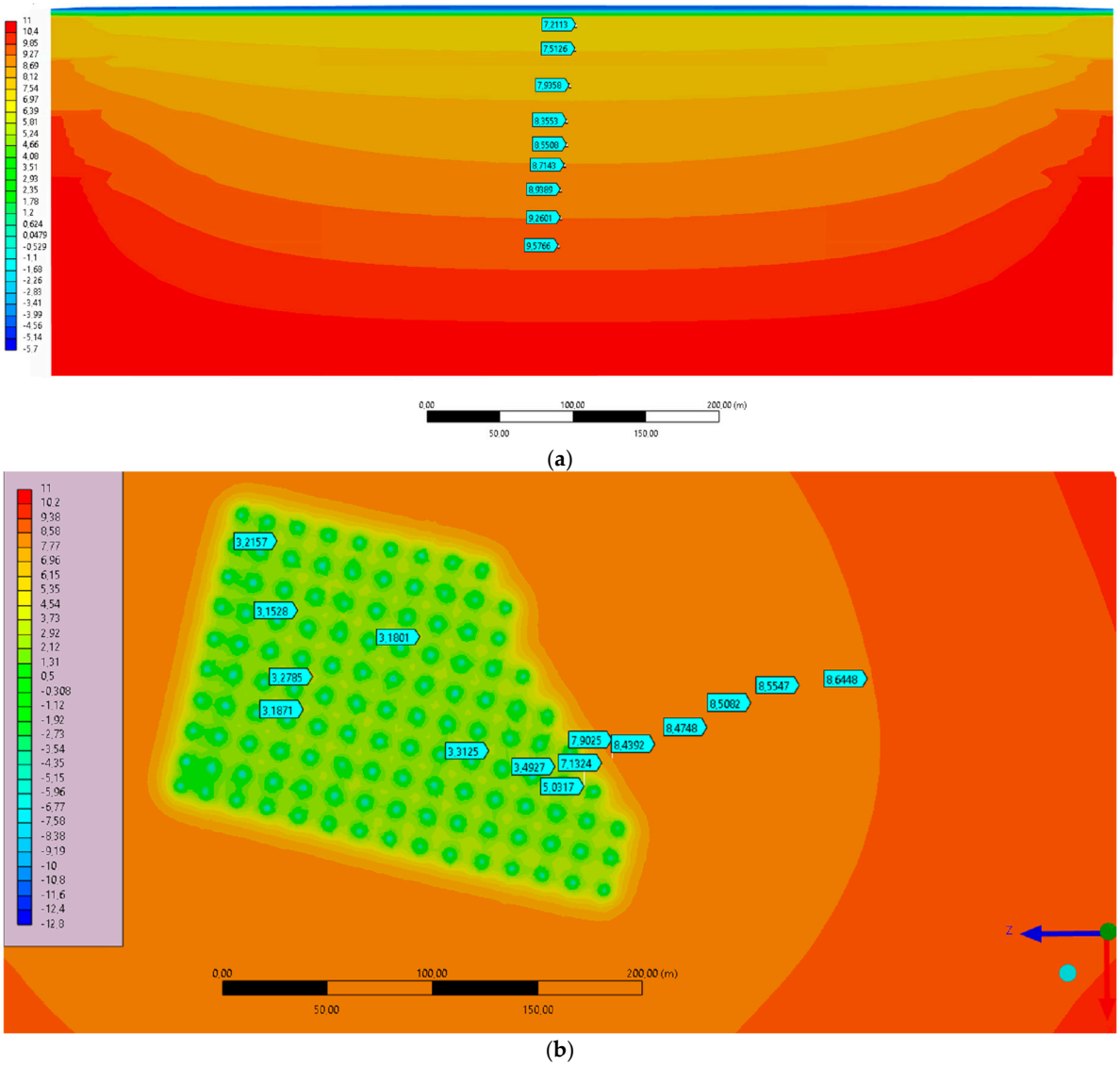

Figure 6. Initial ground temperature assumed in the analysis: (**a**) central cross-section, (**b**) depth of 112.5 m.

The total heat extraction rate was divided among 122 boreholes and then normalised by the surface area of each borehole-wall to obtain the corresponding heat flux required to achieve the above capacities. The temperature gradient along the borehole depth was neglected, and a constant heat flux $\dot{Q}_{BH}$ was prescribed on the inner borehole wall surface.

For the 1-month regeneration scenario, the regeneration period was set in August, coinciding with the annual peak in ambient air temperature and the maximum values of total horizontal solar irradiance (ITH). This represents the most favourable conditions for natural thermal recovery of the shallow geological layers. In contrast, the 6-month regeneration scenario covered the interval from April to November, corresponding to the post-heating season period when the installation remains inactive and the ground is allowed to recover under typical spring–summer–autumn boundary conditions.

The resulting total heat extraction rates $\dot{Q}_{tot}$ for the analysed cases are shown in Figure 7.

Overlapping segments in Figure 7 correspond to identical extraction phases for different scenarios and are shown together for comparison.

Lateral and bottom boundaries were assumed sufficiently distant from the borehole field so that their influence on the simulated temperature field is negligible.

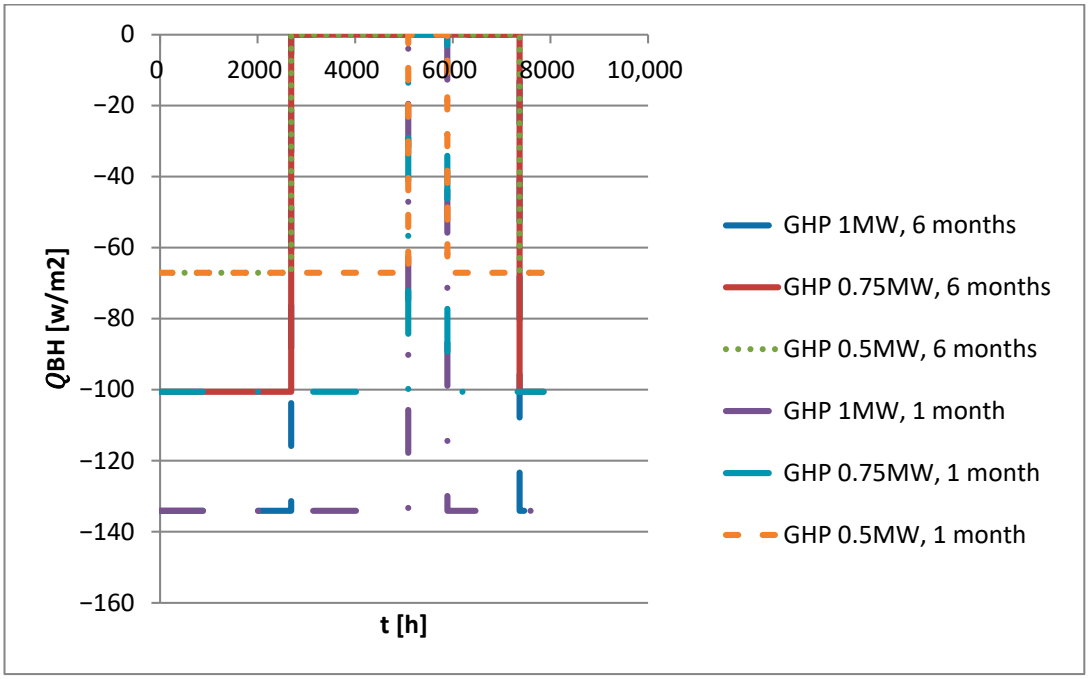

Figure 7. Annual profiles of the heat extraction rates for the analysed cases with corresponding GSHP power and ground temperature regeneration time.

In this study, the heat flux applied at the borehole boundary is not assumed arbitrarily. It follows directly from the required system-scale heat extraction rate and the fixed geometry of the borehole field.

In long-term studies of borehole heat exchangers, it is common to prescribe the heat extraction rate of a borehole or borehole field and to analyse the resulting ground temperature response, rather than to model detailed heat pump operation or fluid temperature control. This approach is particularly appropriate for feasibility assessments focused on long-term thermal balance and ground thermal depletion.

Zeng et al. [22] applied a finite line-source model in which the ground thermal response is calculated for a prescribed heat extraction rate per borehole, with the temperature obtained as the solution of the conduction problem. Al-Khoury et al. [23] analysed the ground response to an imposed borehole heat load using efficient numerical modelling techniques, without explicitly resolving the internal fluid energy balance. More recently, Dehghan et al. [24] proposed a one-dimensional analytical model based on Green's functions, where the long-term heat-transfer rate of a borehole heat exchanger is prescribed to investigate ground thermal behaviour over extended operating periods.

Following this established modelling framework, the present study prescribes the total thermal capacity required by the district heating system (0.50, 0.75 and 1.00 MW) and distributes it over the fixed number of boreholes and their external surface area. The resulting borehole-wall heat flux is therefore uniquely determined by the system capacity and borehole-field geometry, as described in Section 2.3, and is not an independent tuning parameter.

Although changing the applied heat flux would affect the numerical results, such a change would simply reflect a different total extraction capacity. The adopted formulation thus allows a consistent and conservative comparison of district heating-scale loads and their impact on long-term ground thermal depletion.

2.5. Mesh and Results-Independence from Grid Concentration Study

To ensure that the numerical results are not affected by the spatial discretization, a mesh sensitivity analysis [25,26] was performed for the 3D transient thermal model of the borehole field. The computational domain was discretized using unstructured tetrahedral elements with local refinement around the boreholes and at the interfaces between geological layers, where the largest temperature gradients are expected.

Three different meshes were generated: a coarse mesh (M1), a medium mesh (M2), and a fine mesh (M3). The refinement strategy consisted of reducing the element size in the vicinity of the borehole walls and gradually coarsening the grid toward the external boundaries of the domain. Table 2 summarises the main characteristics of the three meshes.

Table 2. Overview of the meshes used in the results-independence from grid concentration study.

Mesh	Number of Elements [-]	Min. Element Size Near Borehole [m]	Typical Element Size in Far Field [m]
M1—coarse	2.3×10^6	0.5	10–12
M2—medium	4.1×10^6	0.3	8–12
M3—fine	6.8×10^6	0.2	6–10

The mesh-independence test was carried out under steady-state conditions for the most demanding extraction scenario (1.00 MW). A constant heat flux corresponding to this load was imposed on all borehole walls, while the same thermal boundary conditions were applied at the ground surface and at the outer boundaries as in the transient simulations.

To quantify the influence of mesh density, seven monitoring points P_1–P_7 were defined, each located at a radial distance of 2 m from the axis of the central borehole, in the middle of each geological layer I-VII (Figure 3).

Table 3 presents the resulting steady-state temperatures obtained at these points for each mesh. The values are representative of the cooled state at the end of the heating season.

Table 3. The influence of mesh density for seven monitoring points P_1–P_7.

Point/Depth [m]	Layer	Temperature M1 [°C]	Temperature M2 [°C]	Temperature M3 [°C]
P_1—15 m	I	4.20	4.01	3.98
P_2—33 m	II	4.05	3.88	3.85
P_3—55 m	III	4.12	3.94	3.90
P_4—96 m	IV	4.33	4.13	4.10
P_5—134 m	V	4.70	4.48	4.45
P_6—155 m	VI	5.05	4.83	4.80
P_7—205 m	VII	5.34	5.08	5.05

The transition from the coarse mesh M1 to the medium mesh M2 leads to temperature changes of up to 0.2–0.3 K at the monitoring points, corresponding to relative differences below approximately 3%. The differences between the medium and fine meshes (M2 vs. M3) are much smaller, not exceeding 0.05–0.06 K at any point (less than 1% relative deviation). This indicates that the solution is effectively grid-independent for mesh densities equal to or higher than M2.

The steady-state case corresponds to the highest thermal gradients and therefore represents the most demanding condition for spatial discretization. The same mesh was subsequently used in all transient simulations.

Considering the balance between accuracy and computational cost, the medium mesh M2 was selected for all transient simulations presented in this work. The remaining numerical uncertainty associated with the spatial discretization is negligible compared with the temperature differences induced by the different extraction loads and regeneration periods discussed in Sections 3 and 4.

Previous studies have shown that excessive heat extraction from borehole fields leads to incomplete seasonal regeneration and cumulative long-term ground cooling [14,24–26].

The present model reproduces these characteristic behaviours, including asymptotic regeneration and persistent post-regeneration temperature deficits, indicating that it captures the dominant physical mechanisms governing long-term ground thermal response.

3. Results

The results are presented in the form of temperature distribution maps for heat extraction rates of 1.0 MW, 0.75 MW, and 0.5 MW and for two regeneration scenarios: 1 month and 6 months. Additionally, the temperature evolution was analysed across six geological layers at depths ranging from 30 m to 250 m, excluding the topsoil layer. Figures 8–13 show the temperature field in the analysed soil. Figures 14–16 show the mean temperature in six layers during the whole year of installation work.

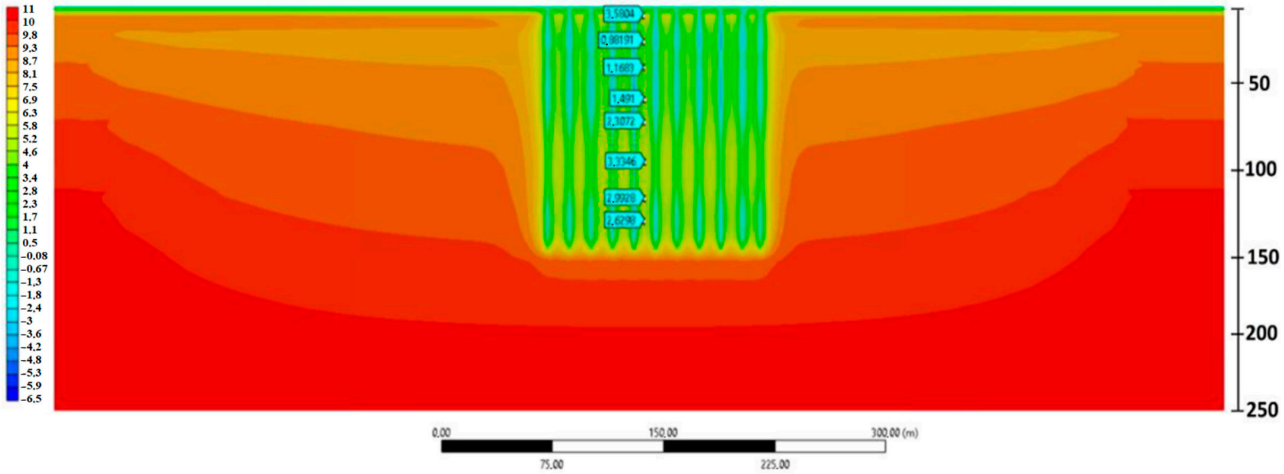

Figure 8. Temperature field distribution for the 1 MW case with a 1-month regeneration period at the centre of the installation.

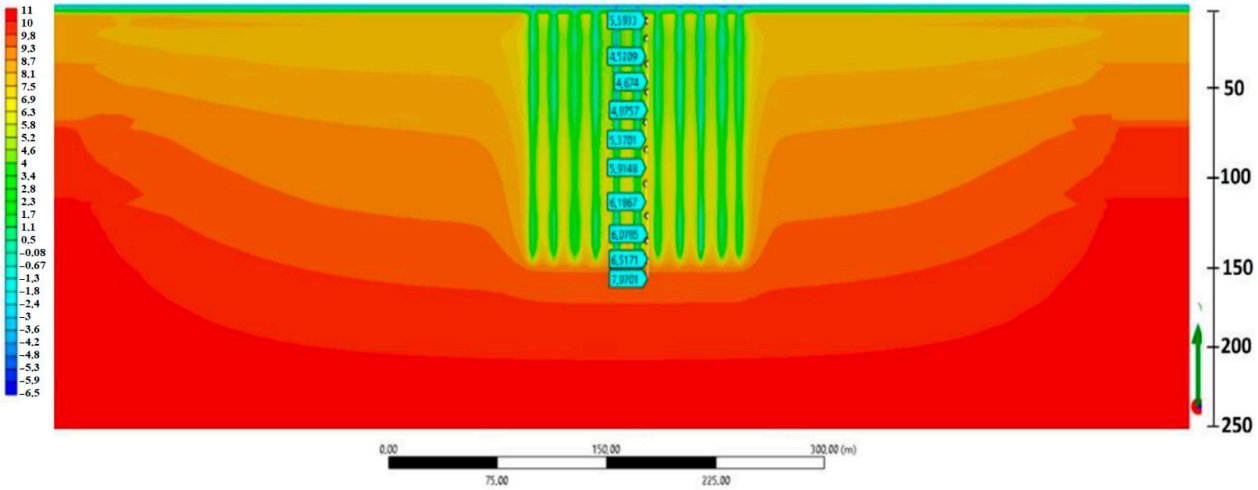

Figure 9. Temperature field distribution for the 1 MW case with a 6-month regeneration period at the centre of the installation.

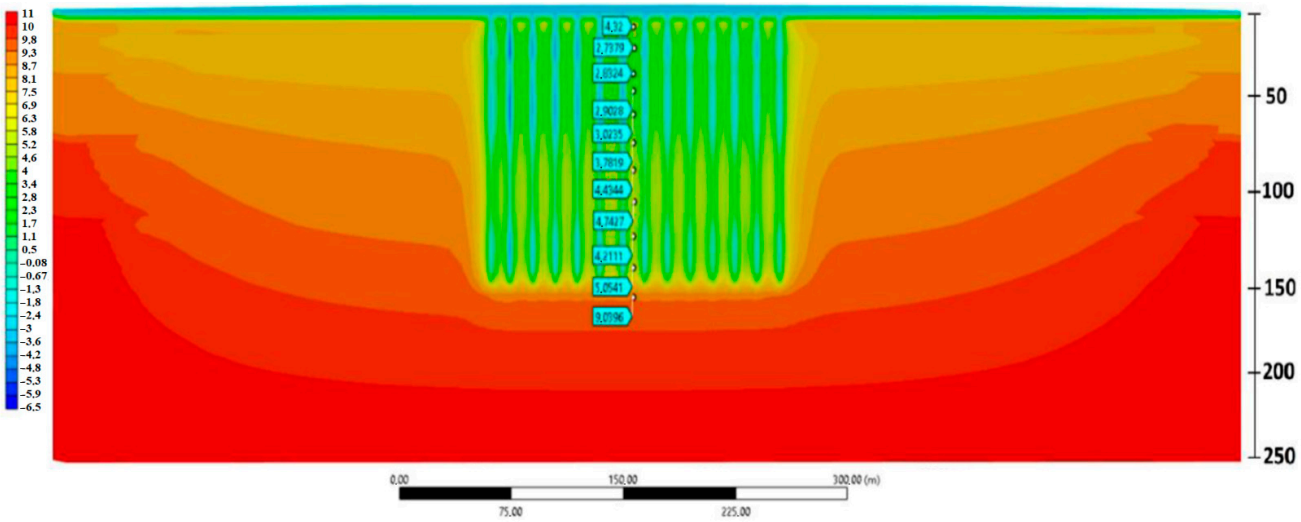

Figure 10. Temperature field distribution for the 0.75 MW case with a 1-month regeneration period at the centre of the installation.

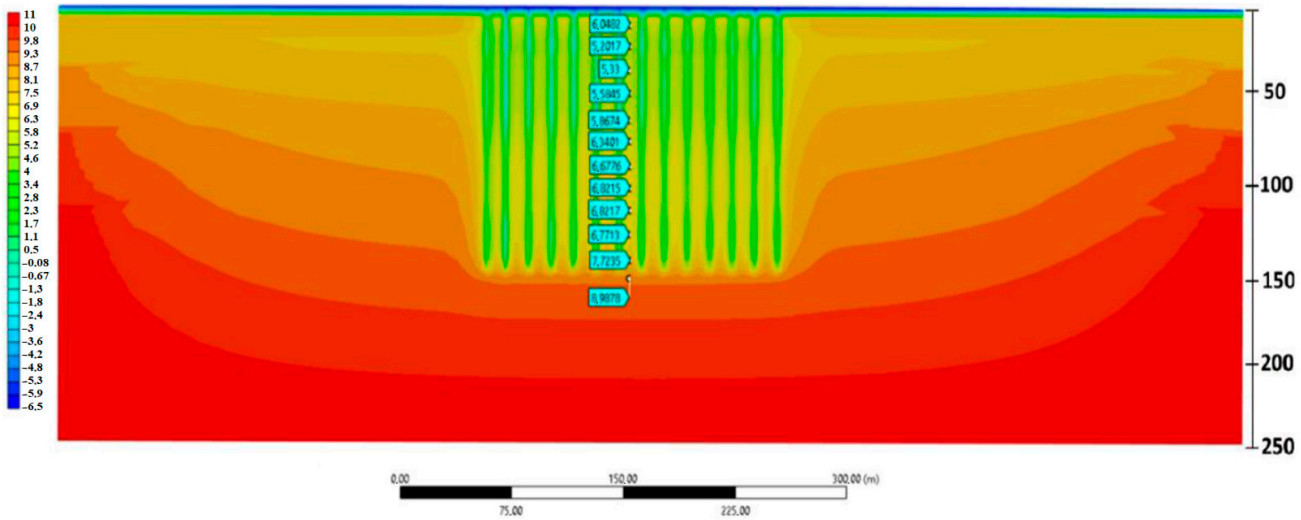

Figure 11. Temperature field distribution for the 0.75 MW case with a 6-month regeneration period at the centre of the installation.

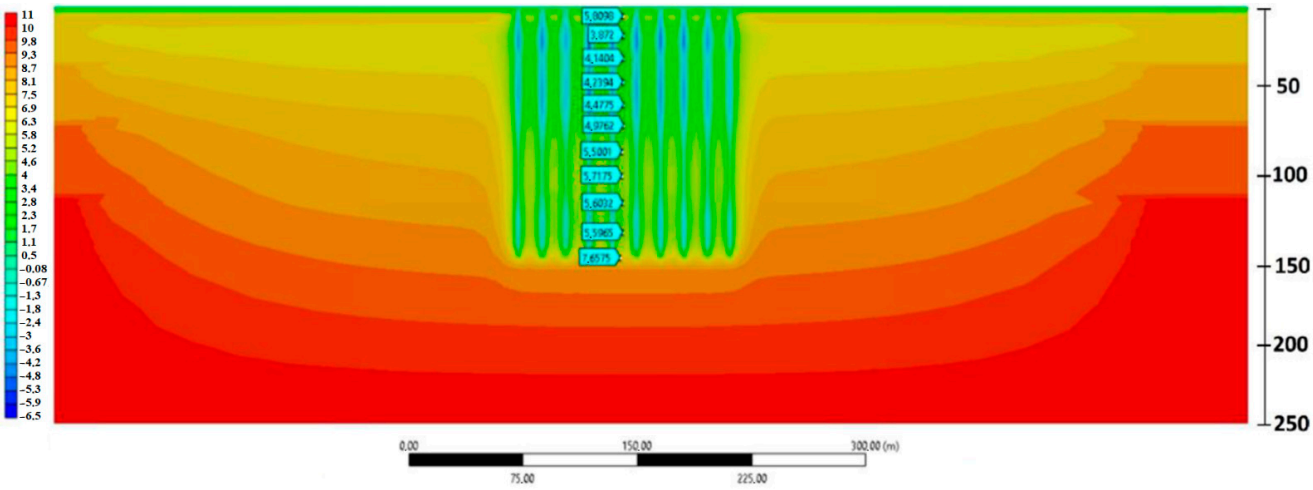

Figure 12. Temperature field distribution for the 0.50 MW case with a 1-month regeneration period at the centre of the installation.

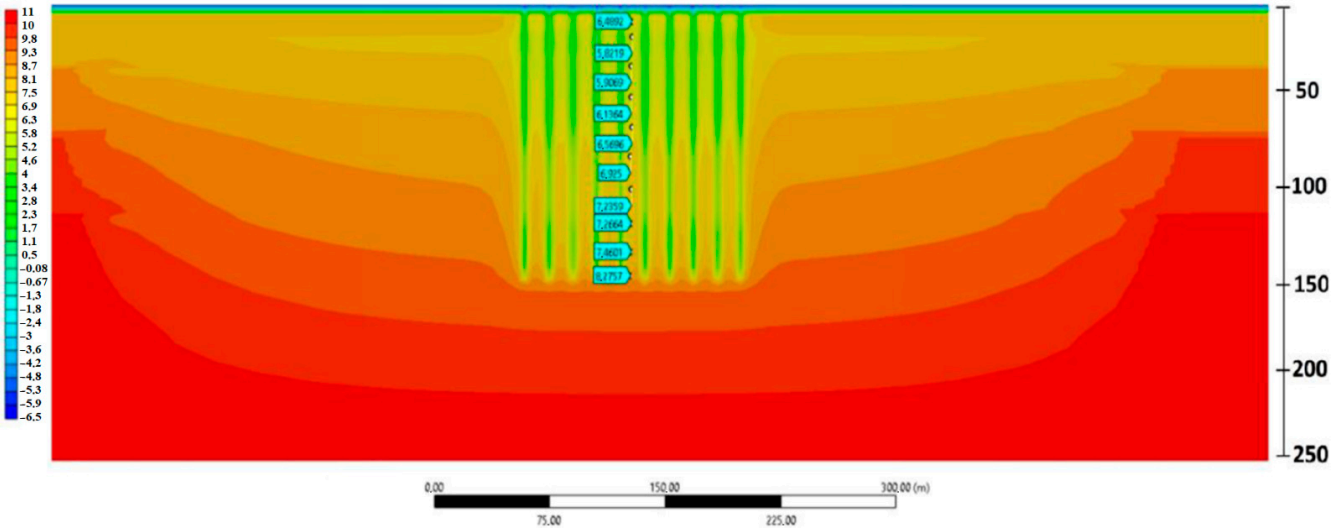

Figure 13. Temperature field distribution for the 0.50 MW case with a 6-month regeneration period at the centre of the installation.

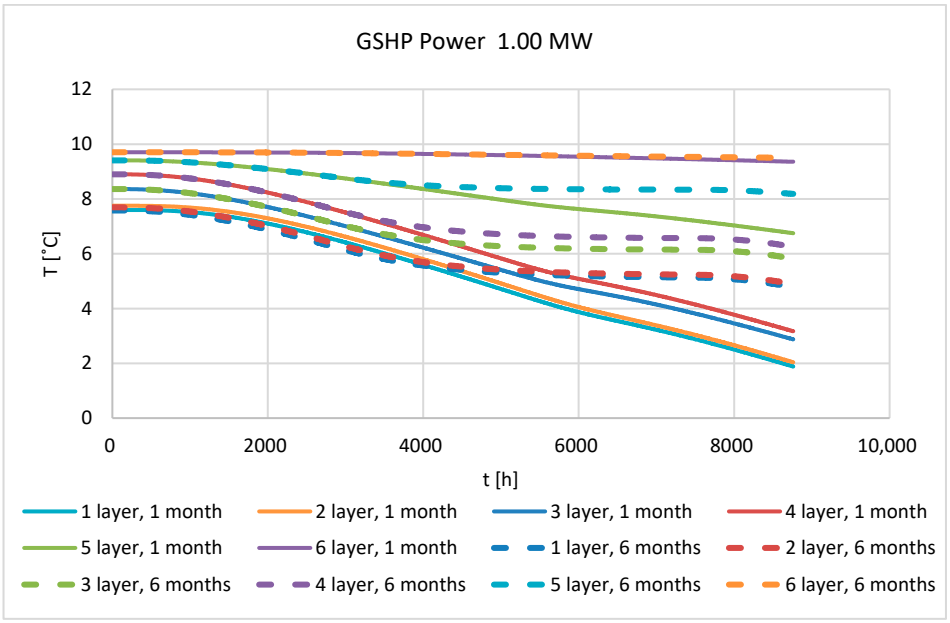

Figure 14. Temperature evolution in six geological layers during system operation at a 1 MW extraction rate.

The presented temperatures represent volume-averaged values for each geological layer.

Additionally, Tables 4–6 show the difference in the temperature values between the initial layer temperature and temperature at the end of regeneration time (1 month—August—and 6 months) for the GSHP 1.00 MW, 0.75 MW, and 0.50 MW.

The numerical simulations clearly show how the ground temperature responds to the imposed heat extraction rates. For the highest load of 1.0 MW, the temperature field exhibits a strong and extensive cooling zone surrounding the borehole cluster. In the central cross-section of the installation (Figure 12), the individual cooling plumes merge into a single, continuous region of significantly reduced temperature, indicating intense thermal interference between neighbouring boreholes. Minimum temperatures in the shallow and mid-depth layers approach 0 °C indicating that the imposed extraction rate exceeds the natural conductive recharge capacity of the subsurface.

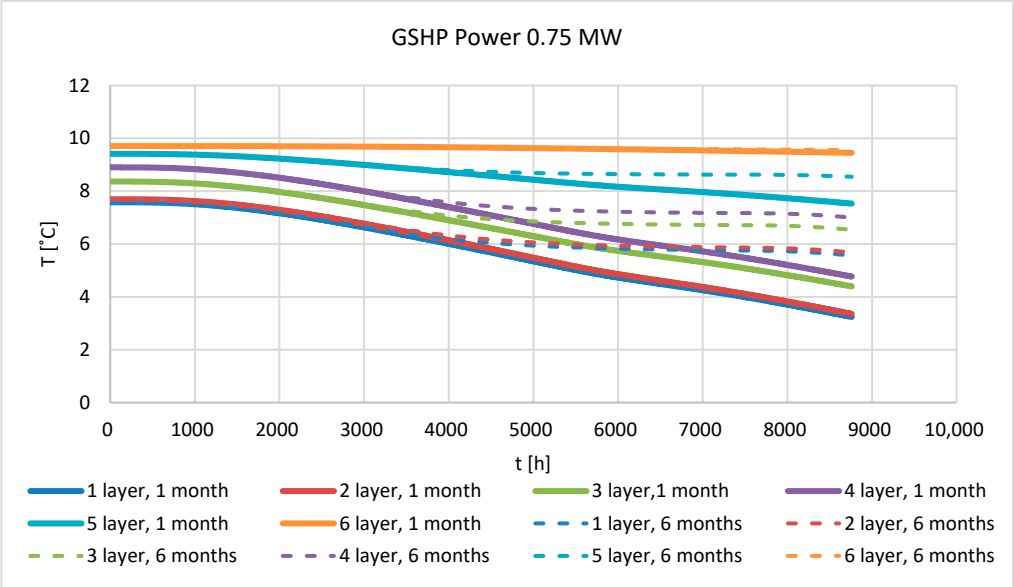

Figure 15. Temperature evolution in six geological layers during system operation at a 0.75 MW extraction rate.

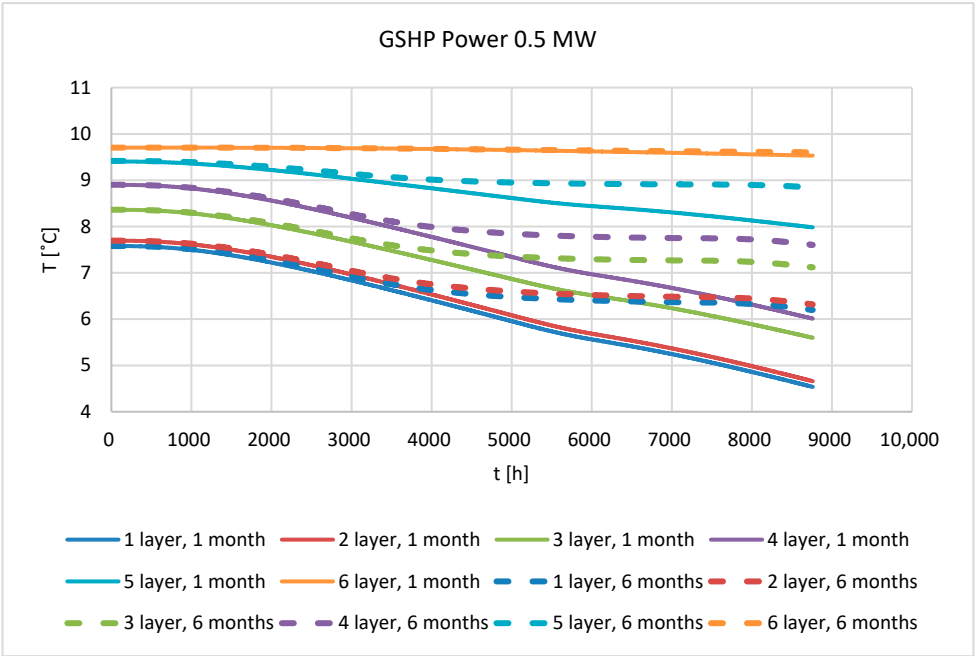

Figure 16. Temperature evolution in six geological layers during system operation at a 0.50 MW extraction rate.

Table 4. The temperature differences between the initial temperature and the temperature after the regeneration [reg.] for the installation at 1.00 MW power.

Layer	1.00 MW (Reg. in August)	1.00 MW (Reg. 6 Months)
1 (30–36 m)	4.22	2.45
2 (36–74 m)	4.27	2.46
3 (74–118 m)	3.60	2.21
4 (118–150 m)	4.13	2.33
5 (150–160 m)	4.27	1.07
6 (160–250 m)	2.04	0.17

Table 5. The temperature differences between the initial temperature and the temperature after the regeneration [reg.] for the installation at 0.75 MW power.

Layer	0.75 MW (Reg. in August)	0.75 MW (Reg. 6 Months)
1 (30–36 m)	2.80	1.82
2 (36–74 m)	2.78	1.83
3 (74–118 m)	2.57	1.65
4 (118–150 m)	2.67	1.73
5 (150–160 m)	1.22	0.79
6 (160–250 m)	0.11	0.12

Table 6. The temperature differences between the initial temperature and the temperature after the regeneration [reg.] for the installation at 0.50 MW power.

Layer	0.50 MW (Reg. in August)	0.50 MW (Reg. 6 Months)
1 (30–36 m)	1.98	1.22
2 (36–74 m)	1.97	1.22
3 (74–118 m)	1.81	1.10
4 (118–150 m)	1.89	1.15
5 (150–160 m)	0.95	0.51
6 (160–250 m)	0.08	0.08

At the depth of 112.5 m (Figure 13), corresponding to the mid-section of the boreholes, the temperature distribution becomes more uniform, but the cooling remains pronounced. Temperatures decrease to approximately 2–3 °C, compared with the initial profile of about 10–11 °C. The one-month regeneration period assigned to August, when ambient temperature and solar irradiance reach their annual maximum, results in only a very limited rebound of roughly 0.5–1.0 °C. This small recovery is insufficient to compensate for the depletion accumulated during the winter extraction period.

The temporal evolution of temperature in six geological layers (Figure 14) further confirms this behaviour. In all analysed layers, from 30 m down to 250 m, the temperature decreases monotonically over the simulation period. The shallow layers show larger short-term fluctuations due to surface boundary conditions, but the deeper layers, which are most relevant for GSHP performance, exhibit the strongest long-term decline. In the interval between approximately 80 m and 200 m, temperatures drop by about 6–8 °C relative to the initial state. Even at 250 m depth, where seasonal variability is normally minimal, a clear downward trend persists. Importantly, none of the layers approach a quasi-steady condition; instead, all exhibit a continuous year-on-year temperature fall, demonstrating that the system is operating in a thermally unsustainable regime.

Extending the regeneration period from 1 month to 6 months (Figure 15) leads to only a modest improvement. During the April–November interval, representing the period immediately following the heating season, the ground temperature rebounds by about 1–1.5 °C. This recovery is larger than in the one-month case but still far smaller than the deficit accumulated during winter. The central region of the borehole field remains significantly cooled, and the trend across all geological layers continues to decline.

The simulations for the reduced extraction rates of 0.75 MW and 0.50 MW (Figures 14–16) show proportionally weaker cooling, but the overall pattern remains unchanged. The temperature drops are smaller, yet the system still does not regenerate fully. The ground temperature after each extraction cycle does not return to the initial value, and the long-term trend remains negative.

The simulations show that the borehole field cannot sustain extraction rates of 0.50–1.00 MW, as all analysed scenarios result in persistent post-regeneration temperature

deficits. At 1.00 MW, the ground cools rapidly and deeply, with insufficient recovery even after six months of non-operation. At 0.75 MW and 0.50 MW, the cooling is slower but still accumulates from year to year. The regenerative capacity of the local geology is therefore far below what would be required for stable long-term district heating-scale operation.

4. Discussion

In accordance with the state-of-the-art literature on borehole heat exchanger (BHE) performance, ground thermal depletion is understood as the long-term, non-recoverable reduction in subsurface temperature caused by excessive heat extraction. Although natural ground regeneration is a slow but theoretically continuous process, the literature shows that this recovery becomes increasingly limited when the annual extraction rate exceeds the regenerative potential of the ground layers. As reviewed by Kirschstein et al. [27], the regeneration process is strongly asymptotic, meaning that initial temperature recovery may be visible, but further rebound becomes progressively slower. When the extraction load is too high, the temperature of the ground does not return to its initial undisturbed value even after extended regeneration periods, which indicates a thermally unsustainable operating regime.

Based on the evidence summarised in the literature [14,27–29], the following conditions are commonly interpreted as indicators of insufficient regeneration and the onset of thermal depletion:

Persistent long-term temperature drops exceeding approximately 0.08–1.22 K after the regeneration period. Several field studies cited by Kirschstein et al. [27] report sustained reductions of ~0.2–1.2 K or more as a clear sign of thermal imbalance within a borehole field.

The temperature differences reported in Tables 4–6 provide a clear picture of how the subsurface reacts to the applied extraction loads. Because the values represent volume-averaged temperatures within each geological layer, they allow for an unambiguous assessment of the thermal state of the ground after regeneration.

For the 1.00 MW case (Table 2), the temperature drops recorded after the one-month regeneration period are substantial. In the upper and middle layers (30–150 m), the ground cools by 3.6–4.3 K relative to the initial state. Even the deepest layer, which is usually less sensitive to seasonal effects, shows a reduction of about 2 K. Extending regeneration to six months improves the situation, but the temperature in the main heat-extraction layers still remains 2.2–2.5 K below the initial profile. These values are large enough to indicate that the system is operating beyond the regenerative capacity of the ground and would continue to cool in subsequent years.

The 0.75 MW scenario (Table 3) exhibits the same tendency, albeit at a slightly reduced magnitude. After one month of regeneration, the upper four layers cool by around 2.6–2.8 K, while the deepest layer shows only a minor change. After six months, the temperature deficit in the upper and middle layers remains at 1.6–1.8 K. Although the deeper layers recover almost fully, the layers responsible for the bulk of heat exchange do not. From the standpoint of long-term operation, such deficits still indicate an unbalanced thermal cycle.

In the 0.50 MW case (Table 4), the cooling is visibly smaller, but the pattern remains the same. After one month of regeneration, the temperature in the upper layers is still roughly 1.8–2.0 K below the initial value. Extending regeneration to six months reduces the deficit to about 1.1–1.2 K. The deepest layer reaches stability almost completely, but the layers that dominate the heat exchange continue to show more than a 1 K difference. Although this scenario performs the best, it still does not meet the criteria for full annual regeneration.

Across all tested loads, the key observation is that none of the extraction rates allow the ground to return to its initial temperature profile after the regeneration period. The

post-regeneration deficits in the active layers, ranging from about 1.1 K at 0.50 MW to more than 2 K at 1.00 MW, are consistent with long-term thermal imbalance described in field studies of overloaded GSHP systems. The behaviour seen here corresponds to a system in which each annual cycle leaves the ground gradually cooler, with no natural mechanism compensating for the deficit.

The analyses indicate that, under the analysed conditions, the borehole field cannot sustain the required extraction rates without long-term thermal imbalance. The system's imbalance is not a local effect around individual boreholes but a volume-wide response of the subsurface, reflected directly in the layer-averaged temperatures.

The long-term behaviour observed here corresponds closely with patterns described in the literature, where ground regeneration is asymptotic and strongly limited once the extraction rate exceeds the subsurface's natural conductive recharge capacity. Indicators commonly used to identify thermal depletion—such as persistent multi-year temperature decline, incomplete seasonal recovery, and the absence of a quasi-steady annual cycle, are all present at the EMPEC Ustka site. For the 1.0 MW case, the deeper layers cool by approximately 6–8 K and recover by only about 1 K even after six months without extraction. This imbalance remains visible even when the extraction rate is reduced to 0.75 MW, where the temperature curves continue to drift downward over time.

The above conclusions are not based solely on the numerical simulations presented in this paper. They are consistent with an independent optimisation study conducted for the same district heating system, which indicated that the available ground heat exchanger capacity is insufficient to act as a standalone heat source and requires complementary air-source operation.

The comparison with air-source heat pumps is made at the system level and does not influence the ground thermal simulations presented in this work.

The analysed regeneration durations represent limiting cases rather than an exhaustive parametric study. The objective was to assess feasibility under favourable assumptions rather than to optimise the system configuration.

The results presented in this study indicate that the analysed ground-coupled ammonia heat pump configuration is thermally unsustainable under the investigated extraction loads and site constraints. Importantly, this conclusion does not invalidate the GSHP concept itself but rather highlights a mismatch between the required district heating-scale load and the regenerative capacity of the local geological formation.

The simulations show that long-term feasibility is governed primarily by the annual thermal balance of the ground. Persistent post-regeneration temperature deficits arise when the imposed extraction exceeds the conductive recharge capacity of the surrounding formations. Consequently, reliable operation can only be achieved by modifying one or more of the governing parameters that control this balance.

In particular, the results indicate that feasibility could be improved by the following:

1. Reducing the annual extraction load to a level compatible with long-term thermal equilibrium, allowing the GSHP to operate as a partial or base-load heat source;
2. Increasing the total ground-side heat-exchange capacity through a larger number of boreholes, greater borehole depth, increased spacing, or a larger available land area, thereby reducing thermal interference;
3. Extending or intensifying regeneration, including the application of active regeneration strategies rather than relying solely on passive conductive recovery; and
4. Adopting hybrid system configurations in which the ground-coupled heat pump is complemented by other low-emission heat sources or thermal storage.

The regeneration durations analysed in this study (1 month and 6 months) were intentionally selected as limiting cases representing favourable boundary conditions. In-

termediate regeneration scenarios would fall between these bounds and, based on the observed trends, would not qualitatively alter the feasibility conclusions for the tested extraction capacities. Meaningful improvement would therefore require structural changes to system configuration rather than minor adjustments of operating periods.

5. Conclusions

A key novelty of this work is that, demonstrating based on real geological data, even a large and densely spaced borehole field may be incapable of sustaining the required heat extraction. This finding challenges the common assumption that GSHP systems can be scaled upward indefinitely and highlights the fundamental importance of ground regeneration dynamics in district heating decarbonization.

Although the numerical model adopts standard engineering simplifications, such as representing each borehole by an equivalent cylindrical exchanger and assuming purely conductive heat transfer, the large-scale cooling trends observed in the results are robust. These simplifications do not alter the main conclusion: the subsurface regeneration rate is insufficient to offset the imposed extraction loads.

The simulations carried out for the EMPEC Ustka site show that the analysed borehole field cannot sustain the heat extraction levels required for the planned high-temperature ammonia heat pump. In all tested variants, 1.00 MW, 0.75 MW, and 0.50 MW, the ground cools noticeably during the heating season and does not return to its initial state during the regeneration period. The post-regeneration temperature differences visible in Tables 2–4, together with the spatial distributions in Figures 8–13, indicate that the annual thermal balance is not achieved even under the most favourable operating conditions.

Although the 0.50 MW case shows the smallest disturbance, the active layers still remain more than 1 K cooler after six months of regeneration. This means that the system would continue to lose temperature over successive years, leading to a gradual decline in heat pump performance. The key limiting factor is the regenerative capacity of the local geology: the heat inflow from surrounding formations is simply too small to compensate for the extraction required for district heating operation.

The numerical model used in this study includes several standard simplifications, such as representing each borehole by an equivalent cylindrical exchanger and assuming purely conductive heat transfer. These choices reduce computational cost but do not change the overall picture. The temperature deficits observed after regeneration occur across the full thickness of the geological layers and are large enough that more detailed modelling would not reverse the main conclusion.

Because the borehole geometry is represented by an equivalent boundary condition, the present model is not intended for accurate estimation of borehole thermal resistance or short-term fluid temperatures.

Based on the numerical results, the analysed GSHP configuration cannot serve as the primary heat source in the analysed configuration. Other low-emission technologies, particularly air-source heat pumps, combined if necessary with photovoltaic systems and thermal storage, are more realistic options for this site and should be considered in the next steps of the system's modernisation.

The negative feasibility outcome reported in this study applies strictly to the analysed configuration and boundary conditions. A reliable long-term operation would require a reduced extraction load, an increased ground heat-exchange capacity, active regeneration, or a hybrid system concept. These findings provide a clear strategic framework for future system redesign and implementation.

Author Contributions: Conceptualisation, M.B. and I.Z.; methodology, I.Z. and T.K.; software, T.K.; validation, J.B., P.J.C.S. and I.Z.; formal analysis, M.B.; investigation, I.Z.; resources, T.K.; data curation, P.J.C.S.; writing—original draft preparation, I.Z.; writing—review and editing, P.J.Z., M.B. and T.K.; visualisation, M.B.; supervision, I.Z.; project administration, T.K. All authors have read and agreed to the published version of the manuscript.

Funding: This research received no external funding.

Institutional Review Board Statement: Not applicable.

Informed Consent Statement: Not applicable.

Data Availability Statement: The data presented in this study are available on request from the corresponding author due to confidentiality agreements with industrial partners.

Acknowledgments: During the preparation of this manuscript, the authors used ChatGPT (OpenAI, GPT-5.1) solely for language checking and minor linguistic corrections. All scientific content, interpretations, analyses, and conclusions were fully written and developed by the authors, who have reviewed and edited the final text and take full responsibility for its content.

Conflicts of Interest: Ireneusz Zagrodzki is employed by the company EMPEC Ustka. The other authors declare no conflicts of interest.

Abbreviations

The following abbreviations are used in this manuscript:

CFD	Computational Fluid Dynamics
GHP	Ground heat pump
GSHP	Ground-source heat pump

References

1. Demir, H.; Gönül, A.; Kayaci, N.; Atayilmaz, Ö.; Ałra, Ö. Thermo-Economicial Optimization of Ground Source Heat Pump with Horizontal Ground Heat Exchangers for a Heating Season in Istanbul: A Case Study. *Am. Soc. Mech. Eng. Fluids Eng. Div. FEDSM* **2014**, *46230*, V01CT16A009. [CrossRef]
2. Lucia, U.; Simonetti, M.; Chiesa, G.; Grisolia, G. Ground-Source Pump System for Heating and Cooling: Review and Thermodynamic Approach. *Renew. Sustain. Energy Rev.* **2017**, *70*, 867–874. [CrossRef]
3. Aresti, L.; Florides, G.A.; Skaliontas, A.; Christodoulides, P. Environmental Impact of Ground Source Heat Pump Systems: A Comparative Investigation From South to North Europe. *Front. Built Environ.* **2022**, *8*, 914227. [CrossRef]
4. Matos, C.; Rosales-Asensio, E.; Carta, J.A.; Cabrera, P. Flywheels in Renewable Energy Systems: An Analysis of Their Role in Managing Intermittency. *J. Energy Storage* **2025**, *122*, 116674. [CrossRef]
5. Jiménez, A.; Cabrera, P.; Fernando Medina, J.; Alberg Østergaard, P.; Lund, H. Smart Energy System Approach Validated by Electrical Analysis for Electric Vehicle Integration in Islands. *Energy Convers. Manag.* **2024**, *302*, 118121. [CrossRef]
6. Rosales-Asensio, E.; Diez, D.B.; Cabrera, P.; Sarmento, P. Effectiveness and Efficiency of Support Schemes in Promoting Renewable Energy Sources in the Spanish Electricity Market. *Int. J. Electr. Power Energy Syst.* **2024**, *158*, 109926. [CrossRef]
7. GeoPortal of Ustka City. Available online: https://gminaustka.e-mapa.net (accessed on 1 January 2026). (In Polish)
8. Yang, Y.L.; Zhang, T.; Chen, Y.; Ma, C.; Cai, G.J.; Wang, C.J. Evolution of Thermal Conductivity for Sand-Clay Composite under One-Dimensional Compression. *Int. J. Heat Mass Transf.* **2025**, *249*, 127243. [CrossRef]
9. Chmengui, H.; Saidia, R.; Hammoodi, K.A.; Choubani, K.; Bouabidi, A.; Kadhim, S.A.; Rashid, F.L.; Almeshaal, M.A. Experimental Investigation of Double Pass Solar Air Heater with Sensible Heat Storage: Effect of Sand Storage Unit Number. *J. Energy Storage* **2026**, *141*, 119353. [CrossRef]
10. Liu, R.; He, W.; Zhou, C.; Hu, Y.; Liu, Y.; Han, T.; Luo, Y.; Wang, M. Study on Quantifying Soil Thermal Imbalance in Shallow Coaxial Borehole Heat Exchangers. *Processes* **2025**, *13*, 2543. [CrossRef]
11. Odoj, M.; Narwojsz, A. *Gis Database of Poland's Hydrogeological Map 1:50,000 First Aquifer Occurrence and Hydrodynamics*; European Union: Warsaw, Poland, 2006. (In Polish)
12. Hyrzyński, R.; Ziółkowski, P.; Gotzman, S.; Kraszewski, B.; Badur, J. Thermodynamic Analysis of the Compressed Air Energy Storage System Coupled with the Underground Thermal Energy Storage. *E3S Web Conf.* **2019**, *137*, 01023. [CrossRef]
13. Badur, J. *Five Lecture of Contemporary Fluid Termomechanics*; IMP PAN Publishing location: Gdansk, Poland, 2005. (In Polish)

14. Bedin, L.; Bazán, F.S.V. On the 2D Bioheat Equation with Convective Boundary Conditions and Its Numerical Realization via a Highly Accurate Approach. *Appl. Math. Comput.* **2014**, *236*, 422–436. [CrossRef]
15. Historical Data of Temperature in Ustka City. Available online: https://www.gov.pl/web/archiwum-inwestycje-rozwoj/dane-do-obliczen-energetycznych-budynkow (accessed on 1 January 2026).
16. Tomaszewska, B.; Dendys, M.; Pająk, L. Analysis of hydrogeological conditions supported by mathematical modelling as the basic stage of investment projects in the field of geothermy. *Biul. Panstw. Inst. Geol.* **2018**, *471*, 179–184. [CrossRef]
17. Banks, D. *An Introduction to Thermogeology: Ground Source Heating and Cooling*, 2nd ed.; John Wiley & Sons: Hoboken, NJ, USA, 2012; pp. 1–526. [CrossRef]
18. Majorowicz, J. Review of the Heat Flow Mapping in Polish Sedimentary Basin across Different Tectonic Terrains. *Energies* **2021**, *14*, 6103. [CrossRef]
19. Szczepański, A.; Haładus, A.; Hajto, M. *Metodyka Analizy Podstawowych Parametrów Hydrogeologicznych Zbiorników Wód Geotermalnych Na Niżu Polskim | Methods of Analysis of Principal Hydrogeological Parameters of Geothermal Aquifers in the Polish Lowlands*; Państwowy Instytut Geologiczny: Warsaw, Poland, 2006; pp. 176–182.
20. (PDF) Atlas Zasobów Geotermalnych Formacji Paleozoicznej Na Niżu Polskim—Atlas of Geothermal Resources of Paleozoic Formations in the Polish Lowlands. Available online: https://www.researchgate.net/publication/275550301_Atlas_zasobow_geotermalnych_formacji_paleozoicznej_na_Nizu_Polskim_-_Atlas_of_geothermal_resources_of_Paleozoic_formations_in_the_Polish_Lowlands (accessed on 25 November 2025).
21. Historical ITC Values in Ustka City in 2023. Available online: https://www.gov.pl/web/archiwum-inwestycje-rozwoj/dane-do-obliczen-energetycznych-budynkow (accessed on 1 January 2026).
22. Zeng, H.Y.; Diao, N.R.; Fang, Z.H. A Finite Line-Source Model for Boreholes in Geothermal Heat Exchangers. *Heat Transf.—Asian Res.* **2002**, *31*, 558–567. [CrossRef]
23. Al-Khoury, R.; Kölbel, T.; Schramedei, R. Efficient Numerical Modeling of Borehole Heat Exchangers. *Comput. Geosci.* **2010**, *36*, 1301–1315. [CrossRef]
24. Dehghan, B.B.; Kukrer, E. A New 1D Analytical Model for Investigating the Long Term Heat Transfer Rate of a Borehole Ground Heat Exchanger by Green's Function Method. *Renew. Energy* **2017**, *108*, 615–621. [CrossRef]
25. Coleman, H. ASME V&V 20-2009 Standard for Verification and Validation in Computational Fluid Dynamics and Heat Transfer (V&V20 Committee Chair and Principal Author). Available online: https://www.researchgate.net/publication/277711647_ASME_VV_20-2009_Standard_for_Verification_and_Validation_in_Computational_Fluid_Dynamics_and_Heat_Transfer_VV20_Committee_Chair_and_principal_author (accessed on 3 December 2025).
26. Celik, I.B.; Ghia, U.; Roache, P.J.; Freitas, C.J.; Coleman, H.; Raad, P.E. Procedure for Estimation and Reporting of Uncertainty due to Discretization in CFD Applications. *J. Fluids Eng. Trans. ASME* **2008**, *130*, 0780011–0780014. [CrossRef]
27. Kirschstein, X.; Ohagen, M.; Reber, J.; Vardon, P.J.; Bishara, N. Regeneration of Shallow Borehole Heat Exchanger Fields: A Literature Review. *Energy Build.* **2024**, *317*, 114381. [CrossRef]
28. Xu, L.; Pu, L.; Zarrella, A.; Zhang, D.; Zhang, S. Experimental Study on the Thermal Imbalance and Soil Temperature Recovery Performance of Horizontal Stainless-Steel Ground Heat Exchanger. *Appl. Therm. Eng.* **2022**, *200*, 117697. [CrossRef]
29. Huang, Y.; Zhao, Z.; Sun, M. Performance Degradation of Ground Source Heat Pump Systems Under Ground Temperature Disturbance: A TRNSYS-Based Simulation Study. *Energies* **2025**, *18*, 3909. [CrossRef]